Theor Appl Climatol
DOI 10.1007/s00704-013-1083-x

ORIGINAL PAPER

Study on the "winter persistence barrier" of Indian Ocean dipole events using observation data and CMIP5 model outputs

Rong Feng · Mu Mu · Wansuo Duan

Received: 8 July 2013 / Accepted: 21 December 2013

Abstract This study investigates the persistence barrier phenomenon associated with positive Indian Ocean dipole (IOD) events during the various phases of its development. The results derived from three observational datasets (the Simple Ocean Data Assimilation, International Comprehensive Ocean–Atmosphere Data Set, and Extended Reconstructed Sea Surface Temperature) indicate that significant winter persistence barriers (WPBs) occur during IOD events, both in its growing and decaying phases. The simulation skill of the 14 models within the Coupled Model Intercomparison Project Phase 5 with respect to persistence barriers was also evaluated and compared with observational data. The results show that although most models were able to simulate the WPB reasonably well during the growing phase, only five models could capture the appropriate WPB during the decaying phase. Further analysis demonstrates that the zonal equatorial gradient of climatological sea surface temperature (SST) and zonal sea surface winds at the equator in the Indian Ocean are very weak in winter, which indicates that the coupling between ocean and atmosphere is weakest in winter and encourages a rapid variation of IOD events and a swift reduction of persistence, favoring the occurrence of WPBs; furthermore, a deep climatological thermocline in winter implies that the subsurface water temperature cannot influence SST readily, and the memory of the subsurface temperature cannot help SST to recover from the loss of persistence during this period, leading to the occurrence of WPBs. In addition, an analysis of the climatological conditions in the outputs from the 14 models shows that those models that can (cannot) capture the winter climatological conditions frequently simulate the WPBs appropriately (poorly). This confirms that the occurrence of the WPB for IOD events may be closely related to particular winter climatological conditions, indicating that the WPB is an inherent property of IOD events.

R. Feng · W. Duan (✉)
LASG, Institute of Atmospheric Physics,
Chinese Academy of Sciences, Beijing 100029, China
e-mail: duanws@lasg.iap.ac.cn

R. Feng
University of Chinese Academy of Sciences, Beijing 100049, China

M. Mu
Key Laboratory of Ocean Circulation and Wave, Institute of Oceanology, Chinese Academy of Sciences, Qingdao 266071, China

1 Introduction

Tropical oceans play an important role in modulating global climate variability. Over recent decades, much attention has been paid to the El Nino–Southern Oscillation (ENSO) phenomenon in the Pacific Ocean (Jin 1997; Picaut et al. 1997; Weiss and Weiss 1999; McPhaden 2003; Duan and Mu 2006, 2009; Mu et al. 2007). Increasing attention has also been paid to the sea surface temperature (SST) in the Indian Ocean, especially to the Indian Ocean dipole (IOD) events (Saji et al. 1999; Webster et al. 1999; Li et al. 2003; Saji and Yamagata 2003a; Annamalai et al. 2005), during which SST anomalies (SSTAs) show an eastern–western seesaw pattern in the tropical Indian Ocean. A positive IOD event exhibits positive SSTAs in the western Indian Ocean and negative SSTAs in the eastern Indian Ocean, with strong easterly winds at the equator (Saji et al. 1999; Webster et al. 1999; Murtugudde et al. 2000; Li et al. 2002, 2003), while a negative IOD event shows the opposite patterns. Phase-locking is a very important characteristic of IOD events. It develops in summer, peaks in autumn and then collapses rapidly in winter (Saji et al. 1999; Webster et al. 1999; Li et al. 2002, 2003; Krishnamurthy and Kirtman 2003; Saji and Yamagata 2003a; Lau and Nath 2004; Shinoda et al. 2004; Cai et al. 2005; Zhong et al. 2005; Behera et al. 2006). A positive IOD event causes significant rainfall in eastern Africa and severe droughts in Indonesia and Australia (Birkett et al.

Published online: 11 January 2014

1999; Ansell et al. 2000; Ashok et al. 2001; Black et al. 2003; Clark et al. 2003; Zubair et al. 2003; Yamagata et al. 2004; Behera et al. 2005). Such IOD events not only modulate the monsoons (Vecchi and Harrison 2004) and affect nearby regions such as eastern Africa, Indonesia, and Australia (Birkett et al. 1999; Ansell et al. 2000; Black et al. 2003), but also influence remote areas such as Europe, northeast Asia, North and South America, and South Africa (Guan and Yamagata 2003; Saji and Yamagata 2003b). Consequently, it is important to predict IOD events successfully months in advance.

The predictability of IOD events has been evaluated using many models (Wajsowicz 2004, 2005, 2007; Luo et al. 2005, 2007; Song et al. 2008; Shi et al. 2012). Shi et al. (2012) assessed the predictive skill of the SST in the Indian Ocean using four different models. They found that the lead time for the skillful prediction of SST in the western Indian Ocean was about 5–6 months, but only 3–4 months for the prediction of SST in the eastern Indian Ocean. The lead time for the prediction of IOD events was about one to two seasons. Similar results have been obtained in other studies (Wajsowicz 2004, 2005; Luo et al. 2005, 2007; Zhao and Hendon 2009). Furthermore, Luo et al. (2007) pointed out that a significant winter predictability barrier exists with regard to IOD events, which may contribute to a poor forecast of these events.

The so-called winter predictability barrier for IOD events is expressed in a phenomenon that, whenever a prediction starts, the forecast skill with respect to IOD events declines rapidly during the boreal winter. Ding and Li (2012) demonstrated that IOD events have the weakest memory of SST variations in winter, which causes the winter persistence barrier (WPB) phenomenon associated with these events. The occurrence of the WPB during IOD events may limit the forecast skill for these events when forecasting across the winter. Consequently, the study of the WPB of IOD events is very important to improve our understanding of the winter predictability barrier of IOD events.

To the authors' knowledge, previous studies focused mainly on the persistence of IOD events either at the east or at the west pole (Wajsowicz 2005, 2007; Ding and Li 2012; Li and Ding 2012), and few studies concentrated on the whole IOD events including the east and west poles. Furthermore, they paid little attention to the persistence of IOD events during their various developmental phases. So far, no studies have investigated the differences between the persistence of IOD events in the growing phase and that in the decaying phase, either in the observational results or in model simulations. Besides, positive IOD events, which are often stronger than their negative counterparts, have larger climate effects, and their frequency of occurrence increases significantly with the climate change of global warming (Ashok et al. 2001; Vinayachandran et al. 2002; Abram et al. 2003; Ashok et al. 2003; Black et al. 2003; Annamalai and Murtugudde 2004; Yamagata et al. 2004; Behera et al. 2005; Hong et al. 2008; Cai et al. 2009; Weller and Cai 2013a). More studies focused on the simulation skill of models for positive IOD events and their climate effects than on that for negative IOD events, reflecting that the foundation of predictability study for negative IOD events may not be solid (Wajsowicz 2004; Tozuka et al. 2007; Liu et al. 2011). Based on these considerations, in this study, we will combine both the east and west poles, with a focus on positive IOD events, to investigate the persistence of IOD events during their different developmental phases using observational datasets and outputs from several models.

The remainder of this paper is organized as follows: The data and methodology are described in Section 2. The nature of the persistence barrier during the different developmental phases of IOD events is explored using observational datasets in Section 3 and model outputs in Section 4. In Section 5, the existence of the WPBs is discussed based on an analysis of climatological conditions. Finally, a summary and discussion is presented in Section 6.

2 Data and methodology

Three observational datasets were used to explore the persistence of IOD events: the Simple Ocean Data Assimilation (SODA 2.2.4, reanalysis data; Carton and Giese 2008), version 2.5 of the International Comprehensive Ocean–Atmosphere Data Set (ICOADS 2.5; Woodruff et al. 2011), and version 3 of the National Oceanic and Atmospheric Administration (NOAA) Extended Reconstructed Sea Surface Temperature (ERSST.v3, monthly SST data; Xue et al. 2003; Smith et al. 2008). The SODA dataset has a resolution of 0.5×0.5° and covers the period 1871–2008, and the SST is taken at a depth of 5 m. The ICOADS has a resolution of 2×2°. As a considerable amount of data are missing in the first 76 years of ICOADS and the data from 2008 onward consist of only preliminary monthly values, only the period from 1876 to 2007 was analyzed. The ERSST dataset ranges from 1854 to 2006, with a resolution of 2×2°, and is derived from the ICOADS dataset. Prior to the analysis, the linear trend of SST was removed from each dataset. The climatological mean annual cycle was calculated using data for the whole period of each dataset, and the SSTAs were then obtained by subtracting the climatological mean annual cycle from the monthly data.

In addition, we also explored the persistence of IOD events using historical outputs from 14 coupled models within the Coupled Model Intercomparison Project Phase 5 (CMIP5) experiments (Table 1; more details are available at http://cmip-pcmdi.llnl.gov/cmip5). The historical runs are simulations of the recent past (from 1850 to at least 2005). The imposed changing conditions (consistent with observations) are as follows: atmospheric composition (including CO_2) due to both anthropogenic and volcanic

Table 1 Brief description of the CMIP5 models used in this study

Model	Institute	Resolution[a]		Time period	N[b]
		Atmosphere	Ocean		
GFDL-CM2p1	NOAA-Geophysical Fluid Dynamics Laboratory	2.0×2.5	0.33×1.0	1,861.1–2,040.12	34
CCSM4	National Center for Atmospheric Research	0.9×1.25	0.27×1.11	1,850.1–2,005.12	38
FGOALS-s2	Institute of Atmospheric Physics (China)	R42	0.5×1	1,850.1–2,004.12	32
CSIRO-Mk3-6-0	CSIRO Marine and Atmospheric Research in collaboration with the Queensland Climate Change Centre of Excellence	T63	0.9375×1.875	1,850.1–2,005.12	45
MRI-CGCM3	Meteorological Research Institute (Japan)	TL159	0.5×1	1,850.1–2,005.12	28
HadCM3	Met Office Hadley Centre	2.5×3.75	1.25×1.25	1,860.1–2,005.12	31
BCC-CSM1.1	Beijing Climate Center, China Meteorological Administration	T42	0.33×1	1,850.1–2,012.12	34
CanESM2	Canadian Centre for Climate Modeling and Analysis (Canada)	T63	0.9375×1.41	1,850.1–2,005.12	27
INM-CM4	Institute for Numerical Mathematics (Russia)	1.5×2	0.5×1	1,850.1–2,005.12	27
IPSL-CM5A-LR	Institut Pierre Simon Laplace (France)	1.895×3.75	0.5×2	1,850.1–2,005.12	16
MIROC5	Atmosphere and Ocean Research Institute, The University of Tokyo; National Institute for Environmental Studies; Japan Agency for Marine-Earth Science and Technology (Japan)	T85	0.5×1.4	1,850.1–2,012.12	27
MPI-ESM-LR	Max Planck Institute for Meteorology	T63	1.5×1.5	1,850.1–2,005.12	18
NorESM1-M	Norwegian Climate Centre	F19	0.267×1.125	1,850.1–2,005.12	35
GISS-E2-R	NASA/GISS (Goddard Institute for Space Studies)	2×2.5	2×2.5	1,850.1–2,005.12	20

[a] Degrees latitude×longitude; ocean resolution at the latitude closest to equator is shown

[b] The numbers of positive IOD events from each model for calculating the autocorrelations

influences, solar forcing, emissions or concentrations of short-lived species and natural and anthropogenic aerosols or their precursors, and land use. These runs could be used to evaluate model performance against the present climate and observed climate change (Taylor et al. 2012).

Finally, we applied the data on temperature at different depths derived from the SODA 2.2.4 reanalysis from 1958 to 2007 (resolution, 0.5×0.5°), and the zonal sea surface winds from ICOADS 2.5 between 1876 and 2007 (resolution, 2×2°) to interpret the existence of the WPBs. In addition, we examined the performance of the 14 models for interpreting the WPBs for IOD events.

In the present study, we used the autocorrelation analysis to measure the persistence of IOD events, that is, the correlation between the IOD index (Saji et al. 1999) for the time series of the start month (a calendar month) and that for the time series of a succeeding lag month (1–12 months after the start month). For each dataset, after filtering out the intraseasonal signals using a 5-month running mean, positive IOD events were selected to compute the autocorrelations of the IOD index at different developmental phases of IOD events using the observations and model outputs.

3 Results from observational datasets

As outlined in the Introduction, we addressed only the persistence of positive IOD events. Positive IOD events usually reverse the sign of the IOD index from negative to positive in winter and from positive to negative in the next winter (Fig. 1). In this study, we investigated the persistence forecast of IOD events over these two winters. These two winters locate respectively in the growing and decaying phases of positive IOD events. The so called growing phase signifies the period from the sign reversal in winter to the peak of the positive IOD event, which typically ranges from December in year (–1; i.e., the year preceding the positive IOD year) to October in year (0; i.e., the positive IOD year); the decaying phase covers the period from the peak of the IOD event to the following sign reversal in winter, which roughly ranges from October in year (0) to February in year (1; i.e., the year following the positive IOD year). In this section, we will discuss about selecting a number of positive IOD events and exploring the persistence during these two phases, before revealing the differences between them.

In Fig. 2a, c, and e, we plot the autocorrelations of the observed IOD index with the start months being April (–1), …, December (–1), January (0), …, December (0), January (1), …, June (1) ("0" indicates the IOD year, while "–1" and "1" indicate the years preceding and following the IOD year, respectively) and the lag months being 1, 2, …, 12 months, where the correlation coefficients significant at the 0.05 level are colored (t test is used for significance testing, and the degree of freedom is the number of IOD events minus 2). Figure 2a shows that, for each start month before March

(0), the persistence of the IOD index makes a reasonably good forecast unless the winter season in the growing phase is encountered; the autocorrelations of the IOD index decrease quickly when they cross the winter season in the growing phase, indicating the occurrence of the WPB. The so-called WPB refers to a dramatic drop in the persistence skill of the IOD index during the boreal winter (Wajsowicz 2007). Similarly, the persistence of the IOD index also provides a reasonable forecast unless the winter season in the decaying phase is encountered, especially for start months after June (0), and the rapid reduction in autocorrelations over this winter period implies the occurrence of the WPB in the decaying phase. Although some uncertainties exist among the three observational datasets regarding the lead times of skillful persistence forecast (or the autocorrelations being larger than 0.6), the WPB phenomenon that occurs in both the growing and decaying phases in the SODA dataset also arises in the ICOADS and ERSST datasets (Fig. 2c, e). To illustrate the WPBs more clearly, we plot in Fig. 2b, d, and f the autocorrelation curves that contain the same information as those in Fig. 2a, c, and e. This shows that, whatever be the start month, the autocorrelations of the IOD index often exhibit a sharp drop during the winter season in the growing or the decaying phase, and cause significant WPBs. These findings imply that, for forecasts of IOD events using the persistence forecast approach, the persistence skill may decline quickly when crossing the boreal winter in the growing and decaying phases due to the existence of the WPBs.

We note that the results derived from the SODA, ICOADS, and ERSST datasets all show significant WPB phenomena, during both the growing and decaying phases of IOD events (Fig. 2). For the SODA dataset, the persistence skill of the IOD index also shows another sharp decline in spring, immediately following the winter season, in both the growing and decaying phases. That is to say, spring persistence barriers (SPBs) also exist and may closely be related to ENSO (Ding and Li 2012). However, the SPB is indistinct in the ICOADS and ERSST datasets during the growing phase of IOD events, indicating uncertainties among the observational datasets. In any case, all these three datasets demonstrate the WPB phenomena of IOD events, both in the growing phase and in decaying phase. It is therefore reasonable that we use these three datasets to address the physics of WPBs for IOD events and evaluate the simulation skill of numerical models with respect to the WPBs.

4 Results from model outputs

The above results, based on observational datasets, illustrate the existence of persistence barriers (especially the WPBs) during positive IOD events. In this section, we will concentrate on the investigation of the performance of CMIP5 models in simulating the WPBs of IOD events. In this study, we chose only 14 CMIP5 models that had often been used to project the properties of IOD events (Cai and Cowan 2013; Weller and Cai 2013a, b; Zheng et al. 2013). The simulation period and the number of selected positive IOD events for each model are listed in Table 1.

Figure 3 shows a comparison between the persistence of the IOD index estimated from the SODA data and that simulated by the 14 CMIP5 models, using the same start and lag months as in Fig. 2. For most models, for each start month before March (0), autocorrelations decrease quickly when they bestride the winter in the growing phase of IOD events, indicating the occurrence of the WPB during this phase, which are similar to the observational results.

When the persistence forecasts of the IOD index are conducted with start months after March (0), which will cross the winter season in the decaying phase of IOD events with a lag time of several months, the patterns of the autocorrelation coefficients of the IOD index in the 14 models vary considerably (Fig. 3). Only five models perform well in simulating the occurrence of the WPB in the decaying phase of IOD events: CanESM2, CSIRO-MK3-6-0, GFDL CM2p1, MIROC5, and MPI-ESM-LR. The autocorrelation curves of these five models also show a sharp drop in the winter of decaying phase, irrespective of the start month (Fig. 4). On the contrary, the remaining nine models fail to capture the main

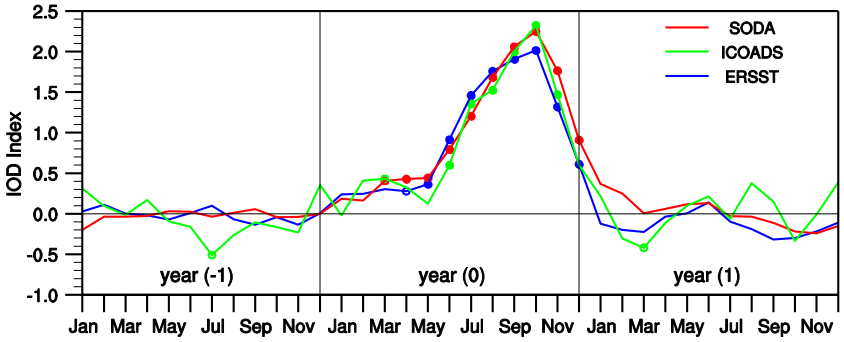

Fig. 1 Composite map of IOD indexes for positive IOD events based on different observational datasets. The *open* (*closed*) *circles* indicate the composite values significant at the 0.1 (0.05) level

characteristics of the persistence barrier in the decaying phase of IOD events and exhibit various patterns of autocorrelation coefficients. Accordingly, the autocorrelation curves show no sharp drop in the winter of the decaying phase for most start months (Fig. 4). It is noteworthy that although the GISS-E2-R model seems to have a rapid autocorrelation drop in the winter of the decaying phase, this drop occurs when autocorrelations having lost their significance at the 0.05 level and is not regarded as a typical WPB phenomenon. It is obvious that most selected CMIP5 models perform poorly in simulating the persistence behavior of the IOD index during the decaying phase of positive IOD events.

In summary, the WPB phenomena were observed during both the growing and decaying phases of IOD events in the three observational datasets, even though many models were unable to capture the characteristics of the persistence barrier in the decaying phase of IOD events. Next, we will explain the climatological conditions favorable for the occurrence of the WPBs and investigate the representation of those conditions in the CMIP5 model outputs.

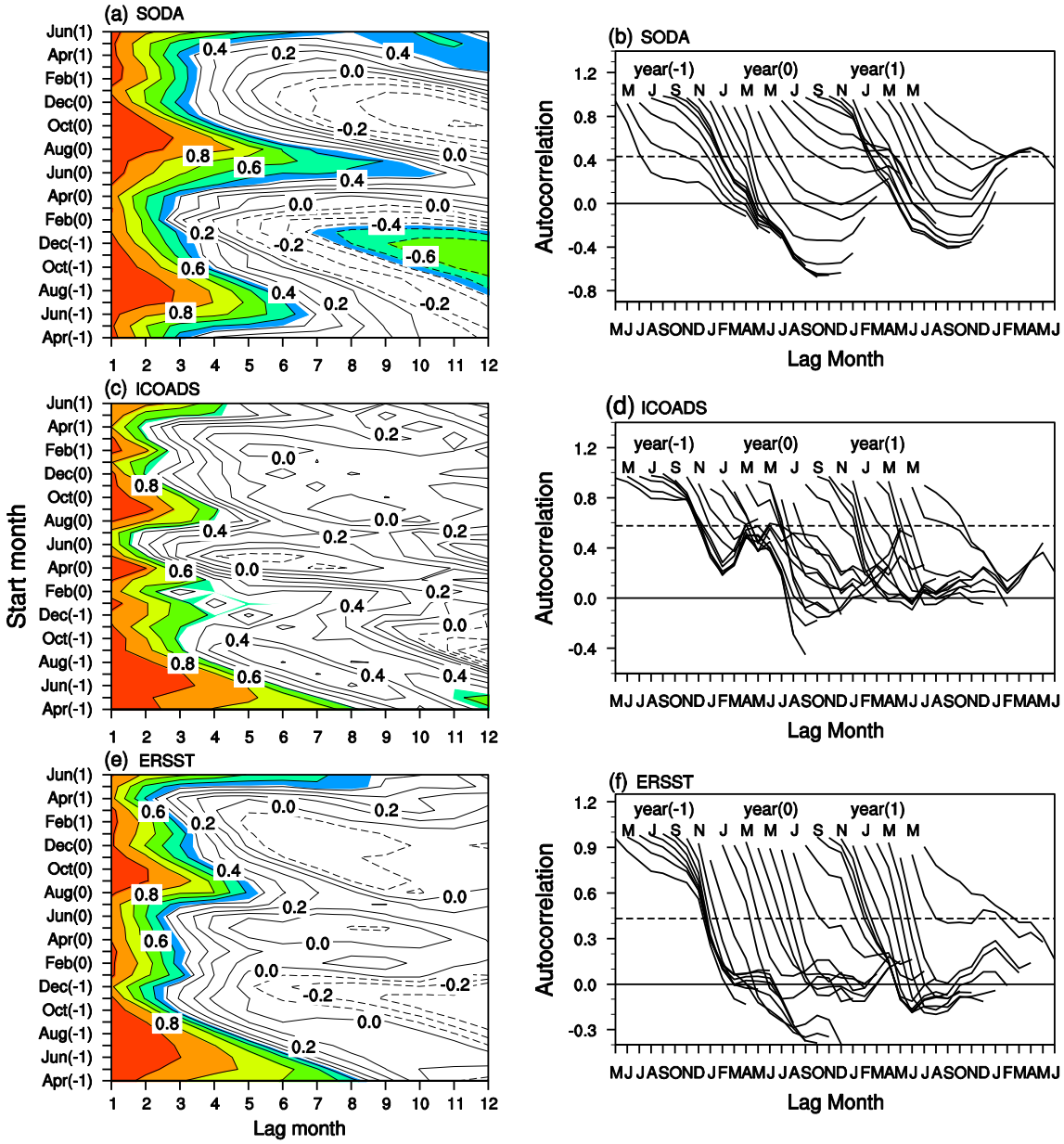

Fig. 2 *Left column*, autocorrelations of the IOD index for (**a**) 21 positive IOD events from the SODA dataset, (**c**) 12 positive IOD events from the ICOADS dataset, and (**e**) 21 positive IOD events from the ERSST dataset as a function of the start and lag months. In (**a**), (**c**), and (**e**), the contour interval is 0.1; autocorrelations significant at the 0.05 level are colored. The *solid* (*dashed*) *lines* denote positive (negative) values. *Right column*, autocorrelation curves of IOD index for positive IOD events from the (**b**) SODA, (**d**) ICOADS, and (**f**) ERSST datasets. The correlation plots have been offset so that the correlations for the same month are lined up along the abscissa. *Letters at the top* indicate the start months. The *horizontal dashed lines* indicate the 0.05 significance level

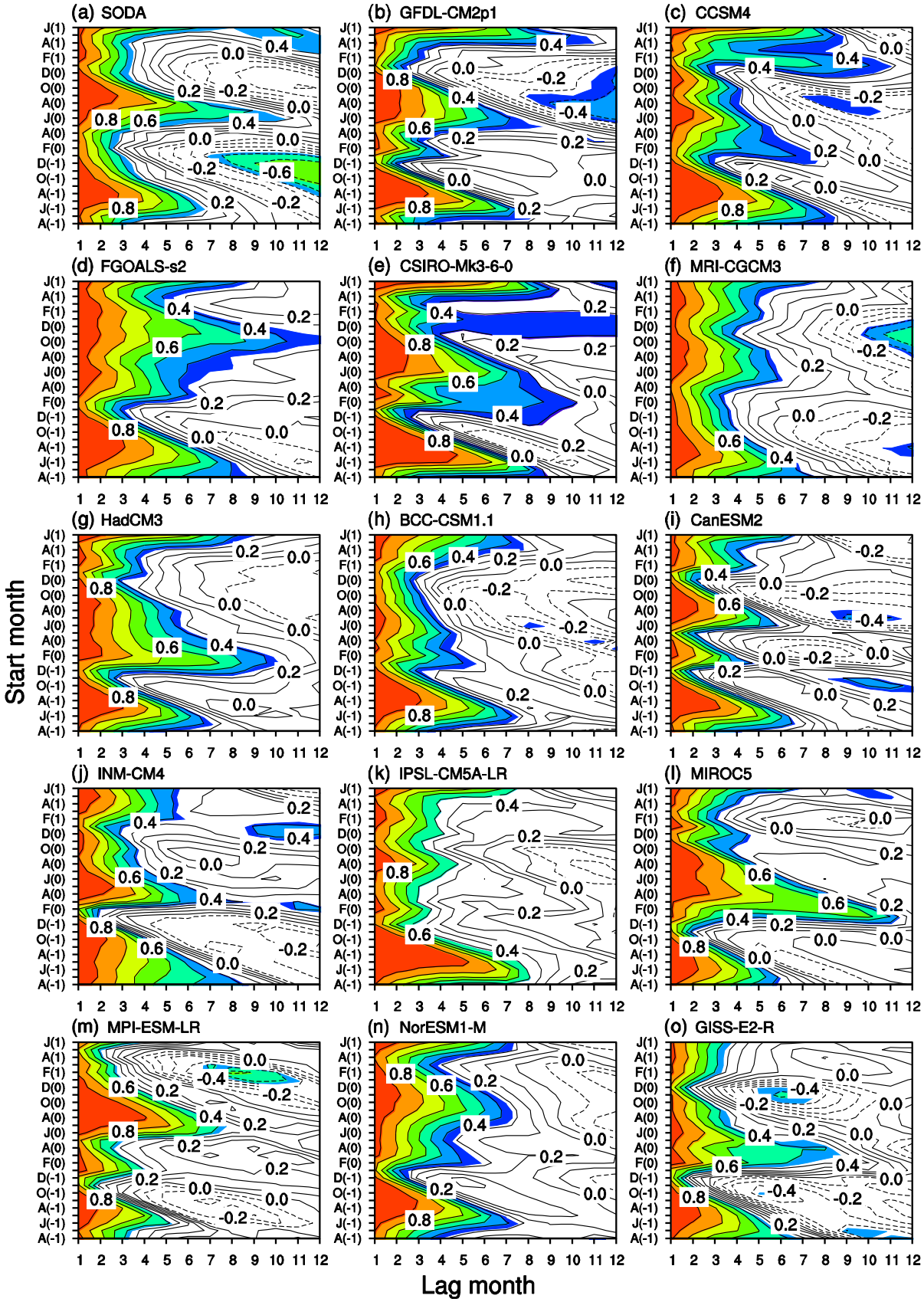

Fig. 3 As in the left column of Fig. 2, but for positive IOD events from the SODA dataset and the outputs of the 14 CMIP5 models

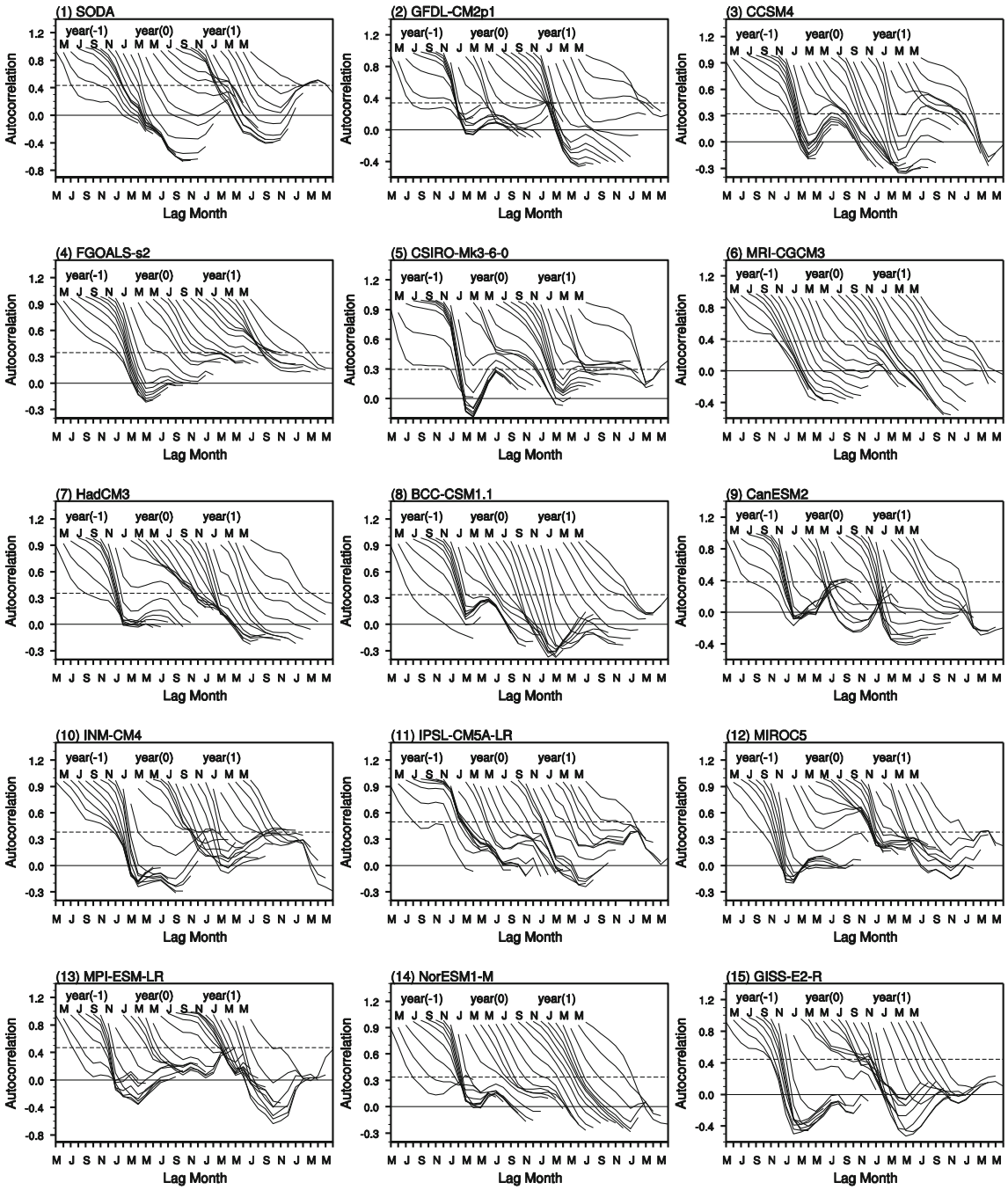

Fig. 4 As in the right column of Fig. 2, but for positive IOD events from the SODA dataset and the outputs of the 14 CMIP5 models

5 Interpretation

In this section, we discuss about the climatological conditions in winter that favor the occurrence of WPBs. Figure 5 shows the zonal equatorial gradient of climatological SST in the Indian Ocean from the three observational datasets. The absolute values of the gradient are very small in winter, which is often accompanied by weak zonal sea surface winds at the equator (Fig. 6). The weak zonal SST gradient and weak zonal sea surface winds at the equator during the winter season indicate that the interaction between the atmosphere and the ocean in winter is weak, and the frail coupled system is influenced much easily by perturbations (initial anomalies of IOD events) during this season. Such perturbations may grow at the fastest possible rate in winter as the atmosphere and ocean become temporally detached (Webster 1995). The fast growth of the perturbations may induce the winter sign reversal of the IOD index easily (Fig. 1), eventually leading to a rapid decline of the persistence of IOD events. Furthermore, the climatological thermocline is very deep in winter,

especially in the eastern Indian Ocean (Fig. 7), which indicates that the vertical temperature gradient in the Indian Ocean is extremely small and the thermocline feedback is weak. This implies that the subsurface water temperature cannot influence SST readily and the memory of the subsurface temperature cannot help SST to recover from the loss of persistence during this period, which finally leads to the occurrence of WPBs.

The above analysis indicates that the WPBs of IOD events are closely related to the rapid variation of the IOD index. To confirm this, we explored the seasonal tendencies of the IOD index during positive IOD events based on the three observational datasets (Fig. 8). As evident from the figure, winter tendencies of the IOD index are very large, in both the growing and decaying phases, indicating a rapid variation of the IOD index in winter and the occurrence of WPBs (Fig. 2). All these confirm that the annual cycle in winter favors the rapid variation of IOD events and reduces their winter persistence, resulting in the WPBs. It is also obvious that, given the effect of the climatological annual cycle, the occurrence of WPBs is closely related to the seasonal phase-locking of IOD events (see also, Saji et al. 1999; Webster et al. 1999; Li et al. 2002, 2003).

Observational data reveal that the climatological conditions in winter strongly favor the occurrence of WPBs. Among the 14 CMIP5 models, some simulate the WPBs well, both in the growing and decaying phases of IOD events, whereas others do not, especially the WPB in the decaying phase. Whether this fact is closely related to the simulation skill of the models for the climatological conditions was addressed by comparing model simulations with observations, and the results are given in Table 2. The comparisons are based on four aspects. The first aspect focuses on the variance of the IOD index that can reflect the phase-locking of IOD events; the second compares the zonal equatorial gradient of climatological SST derived from the observations with that from model outputs; the third contrasts the climatological annual zonal winds at the sea surface; and the fourth is the comparison of the climatological annual thermocline depths. For the variance of the IOD index presented by the models, a "check mark" is used in Table 2 to indicate that the values are smallest during the period from January to April and largest in September or October, which also agree with the observational results (Saji and Yamagata 2003a; Saji et al. 2006; Zhao and Hendon 2009); an "error mark" is used to indicate otherwise. Similarly, a "check mark" symbol indicates that the absolute values of the zonal SST gradient are smallest between January and April and largest in July or August; an "error mark" indicates otherwise. For the patterns of the climatological annual zonal winds and thermocline depth in the models, if the correlation coefficient between the model simulation and observation is larger than 0.5, the similarity is considered significant and the corresponding model is indicated by a "check mark".

From Table 2, it is clear that the five models mentioned previously, GFDL-CM2p1, CanESM2, MPI-ESM-LR, MIROC5, and CSIRO-MK3-6-0, which simulate the WPBs of the observed IOD events well, also describe WPB-related climatological conditions well; the first four models, in particular, perform very well in relation to all the four aspects outlined above. In contrast, the models CCSM4, MRI-CGCM3, BCC-CSM1.1, and INM-CM4 did not capture any characteristics of the climatological conditions; neither did they simulate appropriate WPBs, especially during the decaying phase of IOD events. These results confirm that appropriate simulation of the climatological conditions is vital for the models to represent the WPBs well.

6 Summary and discussion

In this study, we investigated the persistence barrier phenomena associated with positive IOD events, focusing on the growing and decaying phases of these events. The results

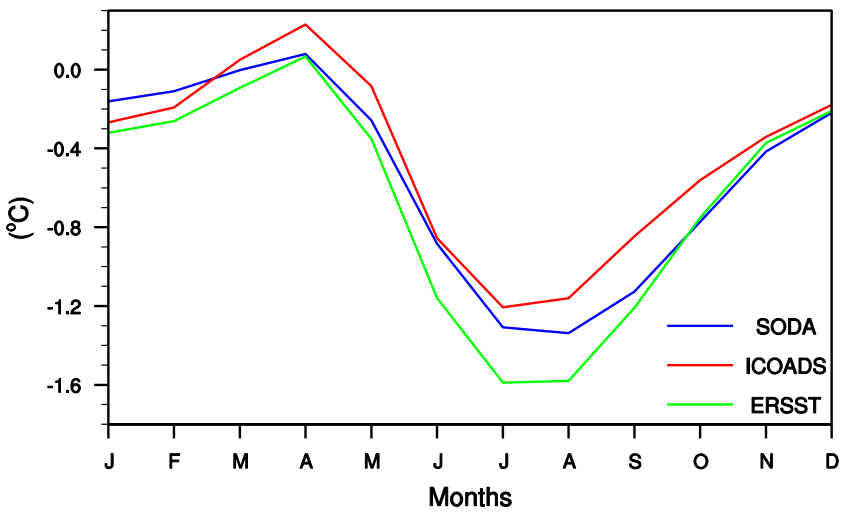

Fig. 5 Zonal equatorial gradient of climatological SST ($T_{west}-T_{east}$) in the tropical Indian Ocean is calculated based on the data from the SODA dataset for the period 1871–2008, the ICOADS dataset for the period 1876–2007, and the ERSST dataset for the period 1854–2006. T_{west} is the SST averaged over 10° S–10° N, 50° E–70° E, and T_{east} is the SST averaged over 10° S–10° N, 90° E–110° E (unit: degrees Celsius)

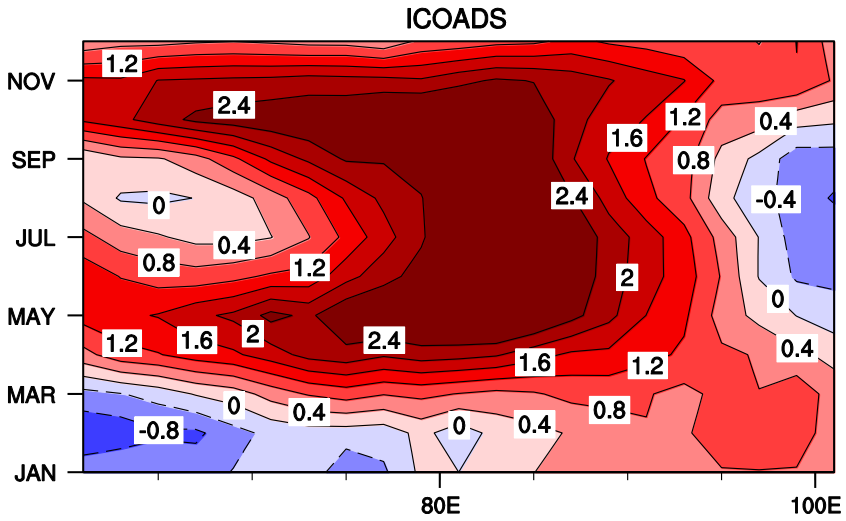

Fig. 6 Time–longitude plot of climatological zonal winds at 10 m at the equator (5° S–5° N) in the Indian Ocean using the ICOADS dataset for the period 1876–2007 (unit: meters per second)

derived from the SODA, ICOADS, and ERSST datasets show that significant WPBs exist in IOD events in both the growing and decaying phases. In the SODA dataset, SPBs are also evident, which follow immediately after the WPBs in both the growing and decaying phases. However, the SPB is not distinct in the growing phase in the ICOADS and ERSST data, which indicates uncertainties among the observational datasets. Nevertheless, the WPBs clearly occur in both the growing and decaying phases of all the three observational datasets; therefore, we focused mainly on the analysis of the WPBs of positive IOD events. The simulation skill of the 14 CMIP5 models was also assessed with respect to persistence barriers and compared with the observational results. The results show that the WPB in the growing phase is well simulated by most models. However, only five models could simulate the appropriate WPB during the decaying phase.

Climatological conditions were also investigated to determine why the persistence barrier tends to occur in winter. The climatological zonal SST gradient and zonal sea surface winds at the equator are very weak in winter, which indicates that the interaction between the atmosphere and the ocean is weak during this period. The frailest tropical coupled system during winter favors the rapid variation of IOD events and a swift reduction of persistence. Furthermore, the climatological thermocline in winter is very deep, especially in the eastern Indian Ocean. This implies that the subsurface water temperature cannot influence SST readily, so the memory of the subsurface temperature cannot help SST to recover from the loss of persistence during this period, which leads to the occurrence of WPBs. In addition, from the analysis of the climatological conditions in the outputs of the 14 models, we found that models GFDL-CM2p1, CanESM2, MPI-ESM-LR, MIROC5, and CSIRO-MK3-6-0, which simulated the WPBs well, also captured the climatological conditions well; in contrast, the models CCSM4, MRI-CGCM3, BCC-CSM1.1, and INM-CM4, which simulated the WPBs poorly, especially in the decaying phase, were unable to simulate appropriate climatological conditions in the Indian Ocean. These results suggest

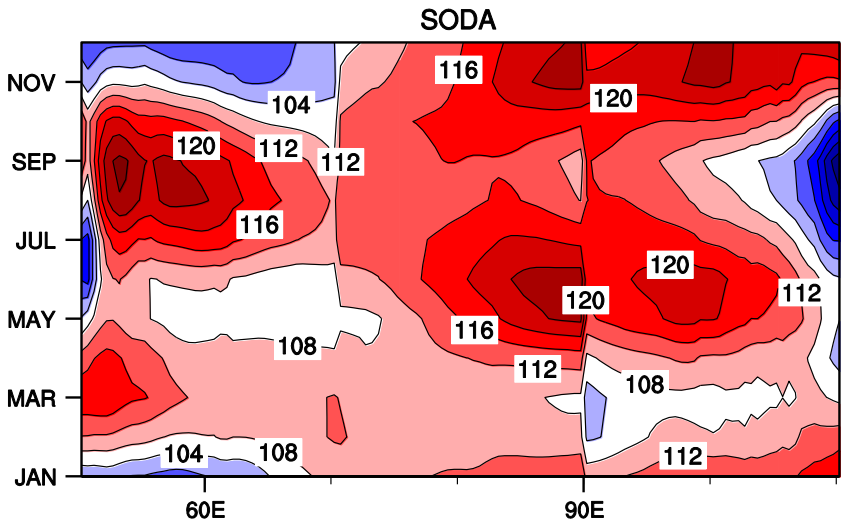

Fig. 7 Time–longitude plot of the climatological thermocline depth (20 °C isotherm) in the tropical Indian Ocean based on the SODA dataset for the period 1958–2007. The thermocline depth at the west pole (50° E–70° E) is averaged between 10° S and 10° N, and that at the east pole (90° E–110° E) is averaged between 10° S and 0° N to emphasize the characteristics at the poles of IOD events. The thermocline depth in other longitude sectors is averaged between 5° S and 5° N (unit: meters)

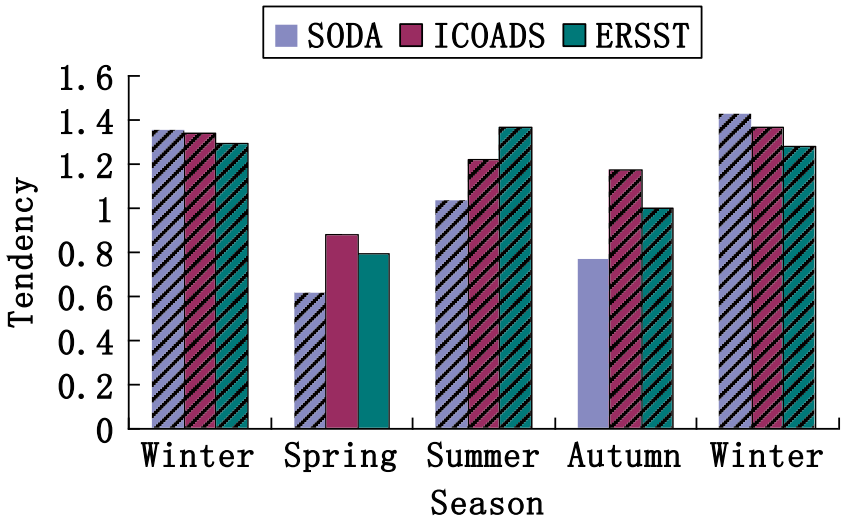

Fig. 8 Composite plot of the absolute values for seasonal tendencies of IOD index based on 21 positive IOD events from the SODA dataset ranging from 1871 to 2008, 12 positive IOD events from the ICOADS dataset ranging from 1876 to 2007, and 21 positive IOD events from the ERSST dataset ranging from 1854 to 2006. The first (second) winter indicates the winter in the growing (decaying) phase. The *bars* masked with oblique lines indicate the values significant at the 0.1 level, by *U* test

that appropriate simulation of the climatological conditions in the Indian Ocean is essential for the reliable simulation of the WPBs of IOD events by the models.

An analysis of the persistence also revealed an SPB phenomenon associated with IOD events, as did previous studies, which argued that the SPB results from the effect of ENSO in the tropical Pacific Ocean (Ding and Li 2012). In the present study, as uncertainties exist in both the observational and the model descriptions of the SPB, we focused mainly on the WPB. Furthermore, the combination of the east and west poles of IOD events in the analysis of persistence, instead of considering only one pole as in previous studies, has reflected the characteristics of persistence at both poles. In addition, previous studies seem to emphasize the occurrence of the winter predictability barrier in the decaying phase (Luo et al. 2007), but we found WPBs in both the growing and decaying phases, which indicates that winter predictability barrier may also exist in the growing phase of IOD events and needs more attention in the future studies.

The above results were derived from the 14 CMIP5 models that had often been used in previous studies. Actually, about a total of 50 models are included in the CMIP5. For other models, we will explore the persistence of IOD events according to the demands of future research. In any case, the prediction of IOD events is an unresolved problem. In this paper, we have revealed the WPB phenomena associated with IOD events using several CMIP5 models and presented an explanation of its physical mechanism. It is commonly agreed that the frailty of the winter ocean–atmosphere coupling in the Indian Ocean favors the fast growth of perturbations and may easily induce a winter sign reversal of the IOD index, finally resulting in the loss of persistence skill and the occurrence of the WPB phenomenon. It is inferred that the WPB often occurs during the transition phase of IOD events and is related to its weak signals

Table 2 Similarity between model outputs and observational datasets with respect to the variance of the IOD index, climatological zonal SST gradient, climatological annual zonal winds at 10 m at the equator, and climatological annual thermocline depth in the tropical Indian Ocean

Model	Variance	Zonal SST gradient	Zonal winds (observation and model)	Thermocline depth (observation and model)
GFDL-CM2p1	✓	✓	0.83**** (✓)	0.65**** (✓)
CCSM4	×	×	0.34**** (×)	0.25**** (×)
FGOALS-s2	✓	×	0.38**** (×)	0.31**** (×)
CSIRO-Mk3-6-0	✓	×	0.56**** (✓)	0.48**** (×)
MRI-CGCM3	×	×	0.23**** (×)	0.11**** (×)
HadCM3	×	✓	0.40**** (×)	0.37**** (×)
BCC-CSM1.1	×	×	0.20*** (×)	−0.03 (×)
CanESM2	✓	✓	0.51**** (✓)	0.51**** (✓)
INM-CM4	×	×	0.30**** (×)	0.20**** (×)
IPSL-CM5A-LR	×	×	0.56**** (✓)	0.39**** (×)
MIROC5	✓	✓	0.71**** (✓)	0.60**** (✓)
MPI-ESM-LR	✓	✓	0.77**** (✓)	0.64**** (✓)
NorESM1-M	×	✓	0.51**** (✓)	0.61**** (✓)
GISS-E2-R	×	×	0.67**** (✓)	0.35**** (×)

Agreement between the model output and observation indicated with "check marks", otherwise "error marks".

BCC Beijing Climate Center, *INM* Institute for Numerical Mathematics, *IPSL* Institut Pierre Simon Laplace

****0.001, significant level (correlation coefficient); ***0.01, significant level

(Tang et al. 2004), which indicates that the WPB may be an inherent characteristic of IOD events, and may favor error growth in winter and limit the prediction skill of IOD events. This raises several questions, including the following: How is the persistence barrier related to the growth of the prediction errors and the predictability barrier of IOD events reported by Luo et al. (2007)? Also, what are the roles of initial errors and model errors in the predictability barrier of IOD events? These questions remain unanswered. By conducting predictability studies of IOD events, especially in view of the error growth, these questions can be answered and the dynamical and physical mechanisms of the predictability barrier of IOD events clarified; these studies can also improve our understanding of, and ability to predict IOD events in the future.

Acknowledgments The authors thank two anonymous reviewers for their constructive suggestions and comments that helped in improving the manuscript significantly. This work was jointly sponsored by the National Basic Research Program of China (no. 2012CB955202), the National Public Benefit (Meteorology) Research Foundation of China (no. GYHY201306018), and the National Natural Science Foundation of China (no. 41176013).

References

Abram NJ, Gagan MK, McCulloch MT et al (2003) Coral reef death during the 1997 Indian Ocean dipole linked to Indonesian wildfires. Science 301(5635):952–955

Annamalai H, Murtugudde R (2004) Role of the Indian Ocean in regional climate variability. Earth Clim: Ocean-Atmos Interact 147: 213–246

Annamalai H, Potemra J, Murtugudde R, Mccreary JP (2005) Effect of preconditioning on the extreme climate events in the tropical Indian Ocean. J Climate 18(17):3450–3469

Ansell T, Reason CJC, Meyers G (2000) Variability in the tropical southeast Indian Ocean and links with southeast Australian winter rainfall. Geophys Res Lett 27(24):3977–3980

Ashok K, Guan Z, Yamagata T (2001) Impact of the Indian Ocean dipole on the relationship between the Indian monsoon rainfall and ENSO. Geophys Res Lett 28(23):4499–4502

Ashok K, Guan Z, Yamagata T (2003) Influence of the Indian Ocean dipole on the Australian winter rainfall. Geophys Res Lett 30(15)

Behera SK, Luo JJ, Masson S, Delecluse P, Gualdi S, Navarra A, Yamagata T (2005) Paramount impact of the Indian Ocean dipole on the East African short rains: a CGCM study. J Climate 18(21): 4514–4530

Behera SK, Luo JJ, Masson S, Rao SA, Sakuma H, Yamagata T (2006) A CGCM study on the interaction between IOD and ENSO. J Climate 19(9):1688–1705

Birkett C, Murtugudde R, Allan T (1999) Indian Ocean climate event brings floods to East Africa's lakes and the Sudd Marsh. Geophys Res Lett 26(8):1031–1034

Black E, Slingo J, Sperber KR (2003) An observational study of the relationship between excessively strong short rains in coastal east Africa and Indian Ocean SST. Mon Weather Rev 131(1): 74–94

Cai W, Cowan T (2013) Why is the amplitude of the Indian Ocean Dipole overly large in CMIP3 and CMIP5 climate models? Geophys Res Lett 40:1200–1205

Cai W, Hendon HH, Meyers G (2005) Indian Ocean dipolelike variability in the CSIRO Mark 3 coupled climate model. J Climate 18(10): 1449–1468

Cai W, Cowan T, Sullivan A (2009) Recent unprecedented skewness towards positive Indian Ocean Dipole occurrences and its impact on Australian rainfall. Geophys Res Lett 36(11), L11705

Carton JA, Giese BS (2008) A reanalysis of ocean climate using Simple Ocean Data Assimilation (SODA). Mon Weather Rev 136(8):2999–3017. doi:10.1175/2007MWR1978.1

Clark CO, Webster PJ, Cole JE (2003) Interdecadal variability of the relationship between the Indian Ocean zonal mode and East African coastal rainfall anomalies. J Climate 16(3):548–554

Ding R, Li J (2012) Influence of ENSO teleconnection on the persistence of sea surface temperature in the tropical Indian Ocean. J Climate 25(23):8177–8195. doi:10.1175/JCLI-D-11-00739.1

Duan W, Mu M (2006) Investigating decadal variability of El Nino–Southern Oscillation asymmetry by conditional nonlinear optimal perturbation. J Geophys Res Oceans (1978–2012) 111(C7). doi:10.1029/2005JC003458.

Duan W, Liu X, Zhu K, Mu M (2009) Exploring the initial errors that cause a significant "spring predictability barrier" for El Niño events. J Geophys Res Oceans (1978–2012) 114(C4). doi:10.1029/2008JC004925.

Guan Z, Yamagata T (2003) The unusual summer of 1994 in East Asia: IOD teleconnections. Geophys Res Lett 30(10). doi:10.1029/2002GL016831

Hong CC, Li T, Ho L, Kug JS (2008) Asymmetry of the Indian Ocean dipole. Part I: observational analysis. J Climate 21(18):4834–4848

Jin FF (1997) An equatorial ocean recharge paradigm for ENSO. Part I: conceptual model. J Atmos Sci 54(7):811–829

Krishnamurthy V, Kirtman BP (2003) Variability of Indian ocean: relation to monsoon and ENSO. Q J Roy Meteorol Soc 129(590):1623–1646

Lau NC, Nath MJ (2004) Coupled GCM simulation of atmosphere–ocean variability associated with zonally asymmetric SST changes in the tropical Indian Ocean. J Climate 17(2):245–265

Li J, Ding R (2012) Temporal-spatial distribution of the predictability limit of monthly sea surface temperature in the global oceans. Int J Climatol 33(8):1936–1947. doi:10.1002/joc.3562

Li T, Zhang Y, Lu E, Wang D (2002) Relative role of dynamic and thermodynamic processes in the development of the Indian Ocean dipole: an OGCM diagnosis. Geophys Res Lett 29(23): 2110–2113

Li T, Wang B, Chang CP, Zhang Y (2003) A theory for the Indian Ocean dipole—zonal mode. J Atmos Sci 60(17):2119–2135

Liu L, Yu W, Li T (2011) Dynamic and thermodynamic air–sea coupling associated with the Indian ocean dipole diagnosed from 23 WCRP CMIP3 models. J Climate 24(18):4941–4958

Luo JJ, Masson S, Behera S, Shingu S, Yamagata T (2005) Seasonal climate predictability in a coupled OAGCM using a different approach for ensemble forecasts. J Climate 18(21): 4474–4497

Luo JJ, Masson S, Behera S, Yamagata T (2007) Experimental forecasts of the Indian Ocean dipole using a coupled OAGCM. J Climate 20(10):2178–2190. doi:10.1175/JCLI4132.1

McPhaden MJ (2003) Tropical Pacific Ocean heat content variations and ENSO persistence barriers. Geophys Res Lett 30(9):1480. doi:10.1029/2003GL016872

Mu M, Duan W, Wang B (2007) Season-dependent dynamics of nonlinear optimal error growth and El Niño–Southern Oscillation predictability in a theoretical model. J Geophys Res Atmos (1984–2012) 112(D10). doi:10.1029/2005JD006981.

Murtugudde R, McCreary JP, Busalacchi AJ (2000) Oceanic processes associated with anomalous events in the Indian Ocean with relevance to 1997–1998. J Geophys Res: Oceans 105(C2):3295–3306 (1978–2012)

Picaut J, Masia F, Penhoat Y (1997) An advective–reflective conceptual model for the oscillatory nature of the ENSO. Science 277(5326): 663–666

Saji NH, Yamagata T (2003a) Structure of SST and surface wind variability during Indian Ocean dipole mode events: COADS observations. J Climate 16(16):2735–2751

Saji NH, Yamagata T (2003b) Possible impacts of Indian Ocean dipole mode events on global climate. Climate Res 25(2):151–169

Saji NH, Goswami BN, Vinayachandran PN, Yamagata T (1999) A dipole mode in the tropical Indian Ocean. Nature 401(6751):360–363

Saji NH, Xie SP, Yamagata T (2006) Tropical Indian Ocean Variability in the IPCC twentieth-century climate simulations. J Climate 19(17): 4397–4417

Shi L, Hendon HH, Alves O, Luo JJ, Balmaseda M, Anderson D (2012) How predictable is the Indian Ocean dipole? Mon Weather Rev 140(12):3867–3884. doi:10.1175/MWR-D-12-00001.1

Shinoda T, Alexander MA, Hendon HH (2004) Remote response of the Indian Ocean to interannual SST variations in the tropical Pacific. J Climate 17(2):362–372

Smith TM, Reynolds RW, Peterson TC, Lawrimore J (2008) Improvements to NOAA's historical merged land-ocean surface temperature analysis (1880–2006). J Climate 21(10):2283–2296. doi:10.1175/2007JCLI2100.1

Song Q, Vecchi GA, Rosati AJ (2008) Predictability of Indian Ocean sea surface temperature anomalies in the GFDL coupled model. Geophys Res Lett 35(2), L02701. doi:10.1029/2007GL031966

Tang Y, Kleeman R, Moore A (2004) A simple method for estimating variations in the predictability of ENSO. Geophys Res Lett 31(17): L17205. doi:10.1029/2004GL020673

Taylor KE, Stouffer RJ, Meehl GA (2012) An overview of CMIP5 and the experiment design. Bull Am Meteorol Soc 93(4):485–498

Tozuka T, Luo JJ, Masson S et al (2007) Decadal modulations of the Indian Ocean dipole in the SINTEX-F1 coupled GCM. J Climate 20(13):2881–2894

Vecchi GA, Harrison DE (2004) Interannual Indian rainfall variability and Indian Ocean sea surface temperature anomalies. In Earth's climate: the ocean–atmosphere interaction. Geophys Monogr Ser 147:247–259

Vinayachandran PN, Iizuka S, Yamagata T (2002) Indian Ocean dipole mode events in an ocean general circulation model. Deep Sea Res II: Top Stud Oceanogr 49(7):1573–1596

Wajsowicz RC (2004) Climate variability over the tropical Indian Ocean sector in the NSIPP seasonal forecast system. J Climate 17(24): 4783–4804

Wajsowicz RC (2005) Potential predictability of tropical Indian Ocean SST anomalies. Geophys Res Lett 32(24), L24702. doi:10.1029/2005GL024169

Wajsowicz RC (2007) Seasonal-to-interannual forecasting of tropical Indian Ocean sea surface temperature anomalies: potential predictability and barriers. J Climate 20(13):3320–3343. doi:10.1175/JCLI4162.1

Webster PJ (1995) The annual cycle and the predictability of the tropical coupled ocean-atmosphere system. Meteorol Atmos Phys 56(1-2): 33–55

Webster PJ, Moore AM, Loschnigg JP, Leben RR (1999) Coupled ocean–atmosphere dynamics in the Indian Ocean during 1997–1998. Nature 401(6751):356–360

Weiss JP, Weiss JB (1999) Quantifying persistence in ENSO. J Atmos Sci 56(16):2737–2760

Weller E, Cai W (2013a) Asymmetry in the IOD and ENSO teleconnection in a CMIP5 model ensemble and its relevance to regional rainfall. J Climate 26:5139–5149

Weller E, Cai W (2013b) Realism of the Indian Ocean Dipole in CMIP5 models: the implication for climate projections. J Climate 26:6649–6659

Woodruff SD, Worley SJ, Lubker SJ, Ji Z, Freeman JE et al (2011) ICOADS Release 2.5: extensions and enhancements to the surface marine meteorological archive. Int J Climatol 31(7):951–967. doi:10.1002/joc.2103

Xue Y, Smith TM, Reynolds RW (2003) Interdecadal changes of 30-yr SST normals during 1871–2000. J Climate 16(10): 1601–1612

Yamagata T, Behera SK, Luo JJ, Masson S, Jury MR, Rao SA (2004) Coupled ocean-atmosphere variability in the tropical Indian Ocean. Earth's Clim 147:189–212

Zhao M, Hendon HH (2009) Representation and prediction of the Indian Ocean dipole in the POAMA seasonal forecast model. Q J Roy Meteorol Soc 135(639):337–352. doi:10.1002/qj.370

Zheng XT, Xie SP, Du Y et al (2013) Indian Ocean Dipole response to global warming in the CMIP5 multi-model ensemble. J Climate 26: 6067–6080

Zhong A, Hendon HH, Alves O (2005) Indian Ocean variability and its association with ENSO in a global coupled model. J Climate 18(17): 3634–3649

Zubair L, Rao AS, Yamagata T (2003) Modulation of Sri Lankan Maha rainfall by the Indian Ocean dipole. Geophys Res Lett 30(2):1063. doi:10.1029/2002GL015639